IJST, Transactions of Mechanical Engineering, Vol. 39, No. M2, pp 351-365
Printed in The Islamic Republic of Iran, 2015

MODELLING THE IMPACT OF RADIATIVE HEAT LOSS ON CO_2 EMISSION, O_2 DEPLETION AND THERMAL STABILITY IN A REACTIVE SLAB*

R. S. LEBELO** AND O. D. MAKINDE

Dept. of Mathematics, Vaal University of Technology, Private Bag X021, Vanderbijlpark, 1911, South Africa
Email: sollyl@vut.ac.za
Faculty of Military Science, Stellenbosch University, Private Bag X2, Saldanha 7395, South Africa

Abstract– In this paper, we examine the effects of thermal radiation on CO2 emission and O2 depletion in an exothermic reactive slab of combustible materials with uniform surface temperature. The governing equations for the nonlinear heat and mass transfer problem are derived and solved numerically using Runge-Kutta-Fehlberg method with shooting technique. Numerical expressions for temperature field, CO2 emitted and O2 depleted are derived and utilised to obtain expressions for Nusselt number and Sherwood number at the material surface. The effects of various thermo-physical parameters on the temperature field, CO2 emission and O2 depletion are depicted graphically and discussed quantitatively. Thermo-physical parameters that help to reduce CO2 emission and hence O2 preservation, are identified, including those which help to monitor measures to avoid explosions in spontaneous combustion processes.

Keywords– Reactive slab, CO2 emission, O2 depletion, thermal radiation, numerical simulation technique

1. INTRODUCTION

Internal heat generation in a stockpile of reactive combustible materials or industrial waste such as coal residue, sugarcane baggage, saw dust, etc., may occur due to oxidation chemical reactions [1, 2]. The continuous accumulations of heat in the material leads to thermal ignition with O_2 depletion and CO_2 emission to the ambient environment [3, 4]. A rise in CO_2 emission to the ambient environment is well known as the major cause of global warming and climate change [5]. Meanwhile, thermal radiation occurs whenever a body's temperature is greater than absolute zero. Thermal radiation is defined as an electromagnetic radiation in the wavelength range of 0.1 to 100 microns, and arises as a result of temperature difference between an object's surface temperature and its surrounding temperature [6-8]. A reactive slab can be thought of as a gray-body, because it absorbs part of the radiation incident to it, rather than a blackbody which absorbs completely all wavelengths of thermal radiation incident to it [9]. Reactive slab emits thermal radiation due to exothermic reaction of its composing hydrocarbon material with oxygen, which brings about temperature rise in the slab [10]. One of the properties that characterizes thermal radiation is the total amount of radiation of all frequencies which increase steeply as the temperature rises [11]. Simmie [12] gave an extensive review of chemical kinetic models for the reaction of hydrocarbons with oxygen in combustible materials. It therefore follows that the combustion reaction mechanism, especially of large hydrocarbons, is more complicated and includes many radicals [13]. Moreover, adequate knowledge of the mathematical models of these complex chemical systems is extremely important in assessing the thermal stability property of the materials, climate change indicators, and mitigation strategies [14]. It may also help to develop a long-term action plan for safety of life and

*Received by the editors November 5, 2014; Accepted February 23, 2015.
**Corresponding author

properties. Several authors [15-17] have examined the thermal stability characteristics of a reacting slab with or without reactant consumption using a one-step decomposition kinetics. Makinde et al. [18] presented a numerical study of CO_2 emission, O_2 depletion and thermal decomposition in a reacting slab. The thermal stability of reacting masses in a slab with asymmetric convective cooling was studied by Makinde [19]. Recently, the numerical result for thermal decomposition of reactive materials of variable thermal conductivity and heat loss characteristics in a long pipe was presented by Makinde [20].

In all the earlier studies, the effects of radiative heat loss on CO_2 emission, O_2 depletion and thermal stability criteria for stockpile of reactive combustible materials have been ignored. Our objective in this paper is to extend the earlier studies to include the effects of radiative heat loss on CO2 emission, O2 depletion and thermal stability of rectangular reactive slab of combustible materials. In the following sections, the differential equations governing the problem are obtained and solved numerically using Runge-Kutta-Fehlberg method with shooting technique. Pertinent results are presented graphically and discussed quantitatively with respect to various thermo-physical parameters embedded in the system.

2. MATHEMATICAL MODEL

We consider a rectangular slab of combustible material with a constant thermal conductivity k, and surface emissivity ε. It is assumed that the slab is undergoing an nth order oxidation chemical reaction. In order to simplify the complicated chemistry involved in this problem, a one-step finite rate irreversible chemical kinetics mechanism is assumed between the material and the oxygen of the air as follows:

$$C_iH_j + \left(i + \frac{j}{4}\right) O_2 \rightarrow iCO_2 + \left(\frac{j}{2}\right) H_2O + heat.$$

Following Stefan-Boltzmann law, the radiative heat loss at the material surface to the surrounding ambient is given by $q = \varepsilon\sigma(T^4 - T_0^4)$ and it is assumed to solely take place in the $\bar{y}$ direction as illustrated in Fig. 1 below,

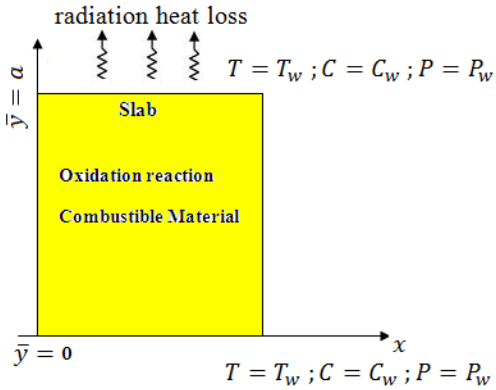

Fig. 1. Geometry of the problem

Following [3-5], the nonlinear differential equations governing the chemical process for the heat and mass transfer problem in the presence of thermal radiation, CO2 emission and O2 depletion can be written as

$$k\frac{d^2T}{d\bar{y}^2} + QA\left(\frac{KT}{vl}\right)^m C^n exp\left(\frac{-E}{RT}\right) - \varepsilon\sigma(T^4 - T_w^4) = 0, \quad (1)$$

$$D\frac{d^2C}{d\bar{y}^2} - A\left(\frac{KT}{vl}\right)^m C^n exp\left(-\frac{E}{RT}\right) = 0, \quad (2)$$

$$\gamma\frac{d^2P}{d\bar{y}^2} + A\left(\frac{KT}{vl}\right)^m C^n exp\left(-\frac{E}{RT}\right) = 0, \quad (3)$$

with boundary conditions:

$$\bar{y} = 0, \quad T = T_w, \quad C = C_w, \quad P = P_w, \tag{4}$$

$$\bar{y} = a, \quad T = T_w, \quad C = C_w, \quad P = P_w, \tag{5}$$

where T is the slab's absolute temperature, C is the O2 concentration, P is the CO2 emission concentration, T_w is the slab surface temperature, C_w is the O2 concentration at the slab surface, P_w is the CO2 concentration at the slab surface, k is the thermal conductivity of the reacting slab, ε is the slab's emissivity ($0 < \varepsilon < 1$), σ is the Stefan-Boltzmann constant ($5.6703\times 10^{-8} W/m^2K^4$), D is the diffusivity of O2 in the slab, γ is the diffusivity of CO2 in the slab, Q is the heat of reaction, $\boldsymbol{A}$ is the rate constant, E is the activation energy, R is the universal gas constant, l is the Planck number, v is the vibration frequency, K is the Boltzmann constant, n is the order of exothermic chemical reaction, and m is the numerical exponent such that $m \in \{-2,0,0.5\}$. The three values taken by the parameter m represent the numeric exponent for sensitized, Arrhenius and Bimolecular kinetics, respectively [8, 10]. The boundary conditions (4) and (5) describe the constant temperature conditions at the base and the top of the reactive slab respectively.

The following dimensionless parameters are introduced to Eqs. (1–5)

$$\left.\begin{gathered} \theta = \frac{E(T-T_w)}{RT_w^2},\ \Phi = \frac{C}{C_w},\ \Psi = \frac{P}{P_w}, \\ \beta_1 = \frac{kRT_w^2}{QEDC_w},\ \beta_2 = \frac{kRT_w^2}{QE\gamma P_w}, \\ \lambda = \left(\frac{KT_w}{vl}\right)^m \frac{QAEa^2(C_w)^n}{kRT_w^2} exp\left(-\frac{E}{RT_w}\right), \\ y = \frac{\bar{y}}{a},\ \ \mu = \frac{RT_w}{E},\ Ra = \frac{\varepsilon\sigma E a^2 T_w^2}{kR}. \end{gathered}\right\} \tag{6}$$

Equations (1–5) take the dimensionless form

$$\frac{d^2\theta}{dy^2} + \lambda(1+\mu\theta)^m \Phi^{\mathrm{n}} \exp\left(\frac{\theta}{1+\mu\theta}\right) - Ra((\mu\theta+1)^4 - 1) = 0, \tag{7}$$

$$\frac{d^2\Phi}{dy^2} - \lambda\beta_1(1+\mu\theta)^m \Phi^{\mathrm{n}} \exp\left(\frac{\theta}{1+\mu\theta}\right) = 0, \tag{8}$$

$$\frac{d^2\Psi}{dy^2} + \lambda\beta_2(1+\mu\theta)^m \Phi^{\mathrm{n}} \exp\left(\frac{\theta}{1+\mu\theta}\right) = 0, \tag{9}$$

$$y = 0,\ \theta = 0, \quad \Phi = 1, \quad \Psi = 1, \tag{10}$$

$$y = 1, \quad \theta = 0, \quad \Phi = 1, \quad \Psi = 1, \tag{11}$$

where λ is the Frank-Kamenetski parameter, μ the activation energy parameter, β_1 the O2 consumption rate parameter, β_2 the CO2 emission rate parameter and *Ra* the radiation parameter. It should be noted further that if the rate of heat generation in the slab exceeds the rate of heat loss to its surrounding, ignition can take place. The dimensionless heat and mass transfer rate at the slab surface are expressed in terms of Nusselt number and Sherwood number, respectively, as

$$Nu = -\frac{d\theta}{dy}(1), \quad Sh_1 = \frac{d\Phi}{dy}(1), \quad Sh_2 = -\frac{d\Psi}{dy}(1). \tag{12}$$

The set of Eqs. (7–9) together with the boundary conditions (10–11) were solved numerically using the Runge-Kutta-Fehlberg method with shooting technique [9]. From the process of numerical computation, the Nusselt number and the Sherwood numbers in Eq. (12) are also worked out and their numerical values are presented graphically.

3. NUMERICAL ALGORITHM

Equations (7-11) were solved using RKF45 method coupled with shooting technique. The shooting technique involves solving a boundary value problem by reducing it to an initial value problem. The process of shooting may use bisection scheme or Newton-Raphson method [21]. The error minimization is attained by use of a small step size when constructing the solutions using Runge-Kutta of order 4. The coupled Runge-Kutta and Shooting methods are embedded in any mathematical software, and in this paper Maple was applied to give solutions graphically. The algorithm gives results to expected accuracy. The following procedure is used, where $\theta = x_1,\ \theta' = x_2,\ \Phi = x_3,\ \Phi' = x_4,\ \Psi = x_5,\ \Psi' = x_6$. It becomes possible to transform Eqs. (7-11) to first order differential equations as follows:

$$
\begin{aligned}
x'_1 &= x_2 \\
x'_2 &= -\lambda(1+\mu x_1)^m (x_3)^n \exp\left(\frac{x_1}{1+\mu x_1}\right) - Ra[(\mu x_1 + 1)^4 - 1] \\
x'_3 &= x_4 \\
x'_4 &= \lambda(1+\mu x_1)^m (x_3)^n \exp\left(\frac{x_1}{1+\mu x_1}\right) \\
x'_5 &= x_6 \\
x'_6 &= -\lambda(1+\mu x_1)^m (x_3)^n \exp\left(\frac{x_1}{1+\mu x_1}\right).
\end{aligned} \tag{13}
$$

Initial conditions are considered as follows:

$$x_1(0) = 0,\ x_3(0) = 1,\ \ x_5(0) = 1,\ x_1(1) = 0,\ \ x_3(1) = 1,\ x_5(1) = 1 \tag{14}$$

4. RESULTS AND DISCUSSION

In this section, the computational results obtained for the model equations in the above section are presented graphically and discussed quantitatively for various values of thermo-physical parameters embedded in the system.

a) Effects of thermo-physical parameter variation on slab temperature profiles

Figures 2-7 illustrate the temperature profiles. Generally, the slab temperature is maximum along the slab centerline region and minimum at the walls satisfying the prescribed boundary conditions. In Fig. 2, we observe that the slab temperature increases with increasing values of λ due to increasing rate of internal heat generation by exothermic chemical reaction. We observe a different case in Fig. 3 where the increase in *Ra* leads to the decrease in temperature. This indicates that the more heat lost due to radiation, the more the temperature of the slab is reduced. The same scenario is observed with Fig. 4. It can be seen that the slab's temperature decreases with increasing *n* and this indicates that increasing the order of reaction in an exothermic reaction results with minimum temperature drop in a reactive slab. Figure 5 illustrates the effects of *m* on temperature. It can be observed that the increase in *m* corresponds to the increase in temperature. The results indicate that exothermic reaction occurs faster during bimolecular reactions (*m* = 0.5) which gives highest temperature profile as compared to Arrhenius (*m* = 0) type of reaction, and that it is slower during sensitized (*m* = -2) chemical reaction. Effect of increasing μ on slab temperature profiles is illustrated in Fig. 6, which indicates that increasing μ results in decrease in temperature. In other words, an increase in the activation energy of the exothermic reaction in a reactive slab lowers the temperature. Figure 7 shows the same scenario, where an increase in β_1 results in a decrease in temperature. When oxygen is consumed in the system, the exothermic reaction is reduced and this causes a drop in the temperature of the slab.

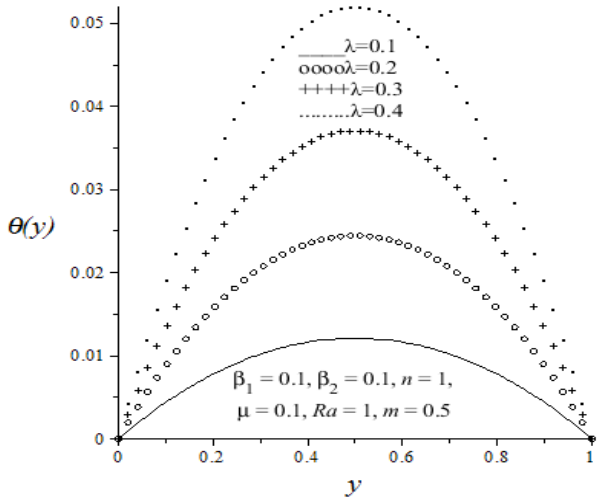

Fig. 2. Effect of increasing λ on slab temperature profiles

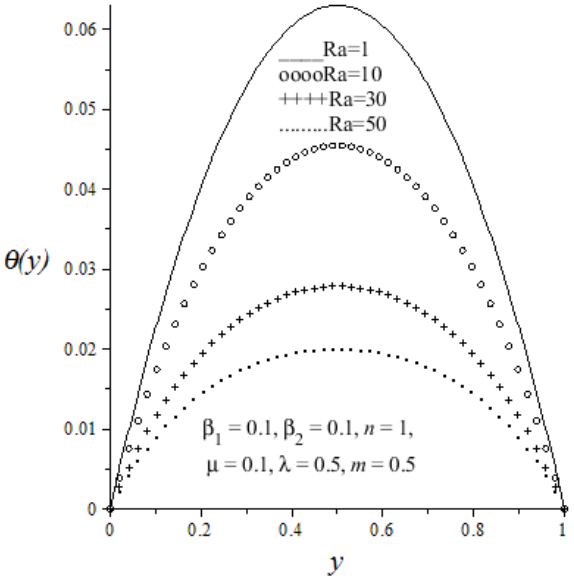

Fig. 3. Effect of increasing *Ra* on slab temperature profiles

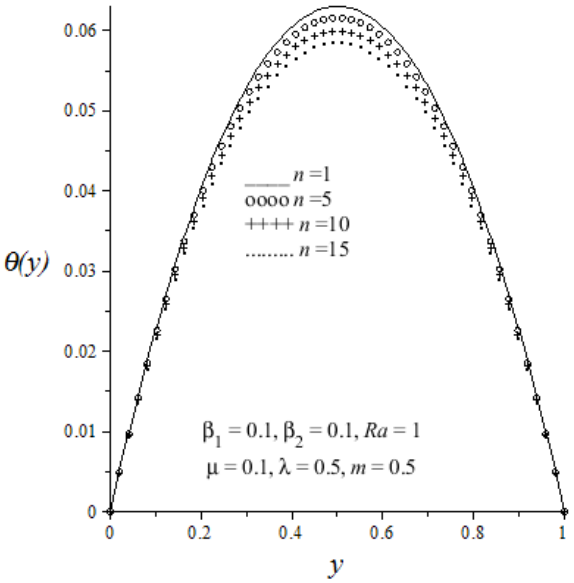

Fig. 4. Effect of increasing *n* on slab temperature profiles

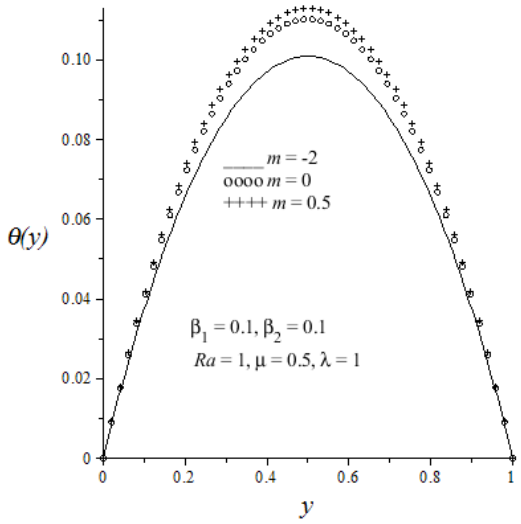

Fig. 5. Effect of m on slab temperature profiles

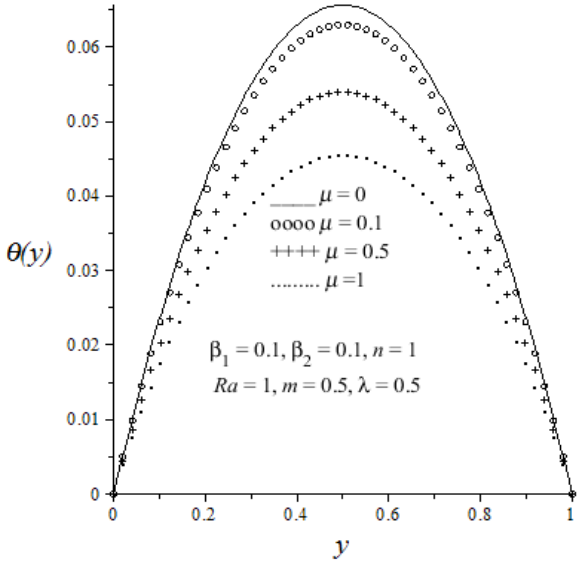

Fig. 6. Effect of increasing μ on slab temperature profiles

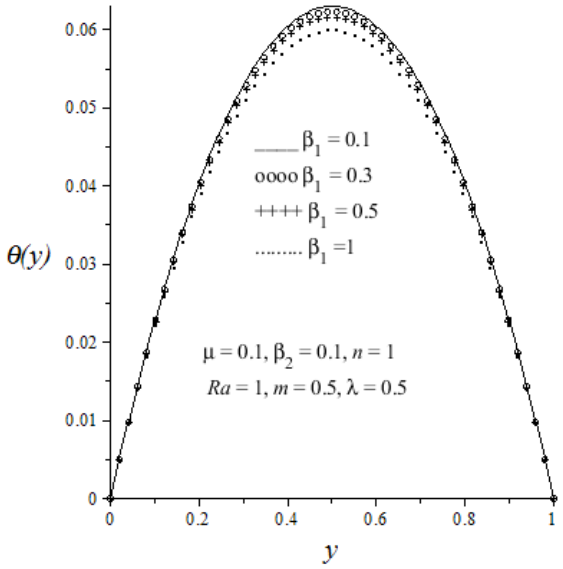

Fig. 7. Effect of increasing β_1 on slab temperature profiles

b) Effects of thermo-physical parameter variation on slab O2 depletion

The effects of parameter variation on slab O2 depletion are demonstrated in Figs. 8 -12. It is interesting to note that the rate of O2 depletion within the slab increases with an increase in the exothermic reaction rate as shown in Fig. 8. As λ increases, more O2 is consumed to generate more heat due to oxidation chemical reaction. From Fig. 9 we observe that as *Ra* is increased, the O2 concentration is increased. This means that the greater the emissivity of slab's surface, the lesser the exothermic reaction and more O2 preservation. The same scenario is observed with Fig. 10, where an increase in *n* results in increase in O2 concentration. It is good to see that increasing the order of chemical reaction favors the O2 conservation. Figure 11 illustrates that an increase in *m* decreases the temperature concentration. It can be observed that more O2 is depleted during bimolecular reaction (m = 0.5). Effect of increasing β_1 is illustrated in Fig. 12. It can be observed that as β_1 is increased, more O2 is depleted. The more O2 consumed in a reactive slab, the more the exothermic chemical reaction is reduced and we can also observe that the temperature of the slab decreases.

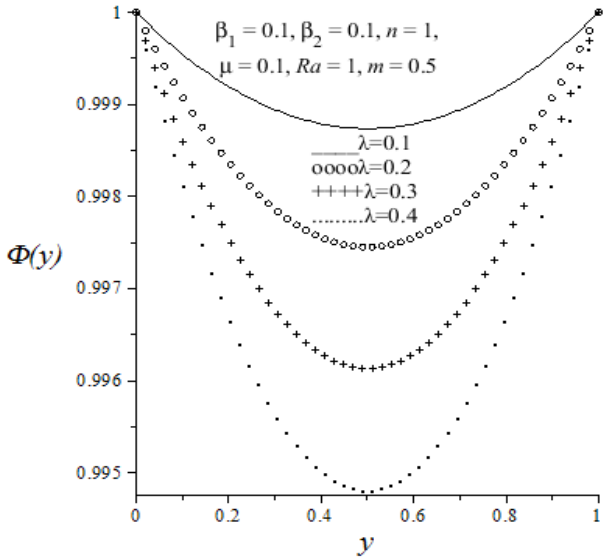

Fig. 8. Effect of increasing λ on slab O2 depletion profiles

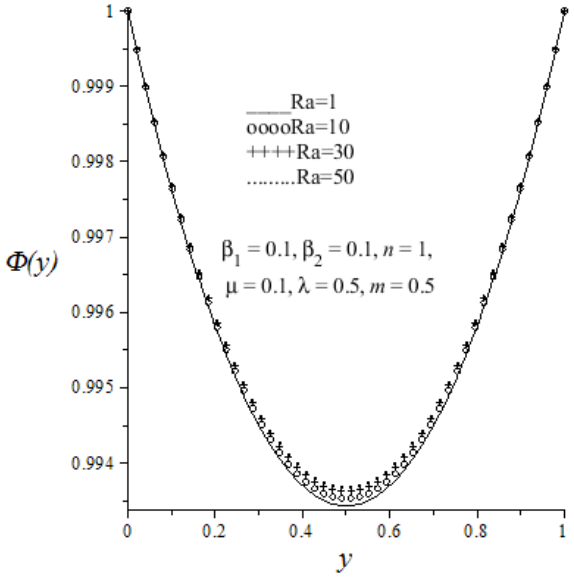

Fig. 9. Effect of increasing *Ra* on slab O2 depletion profiles

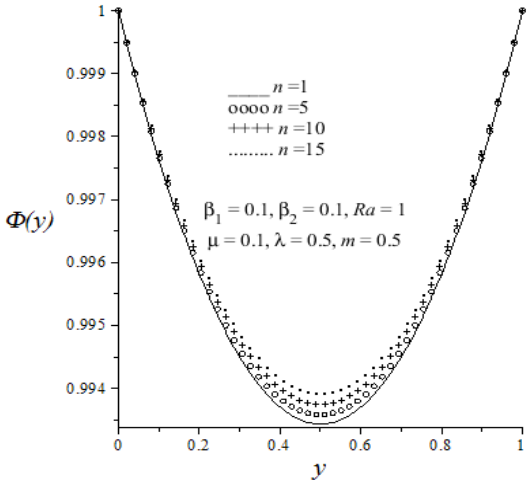

Fig. 10. Effect of increasing *n* on slab O2 depletion profiles

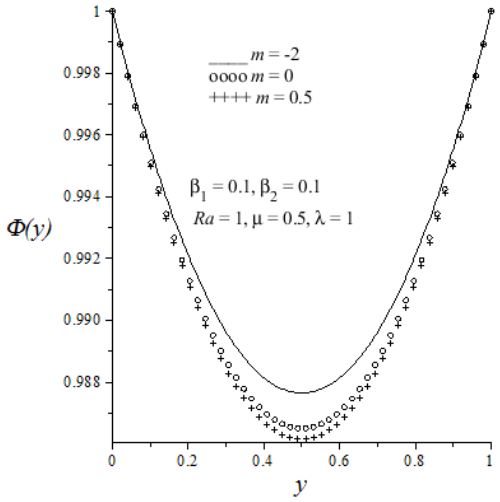

Fig. 11. Effect of *m* on slab O2 depletion profiles

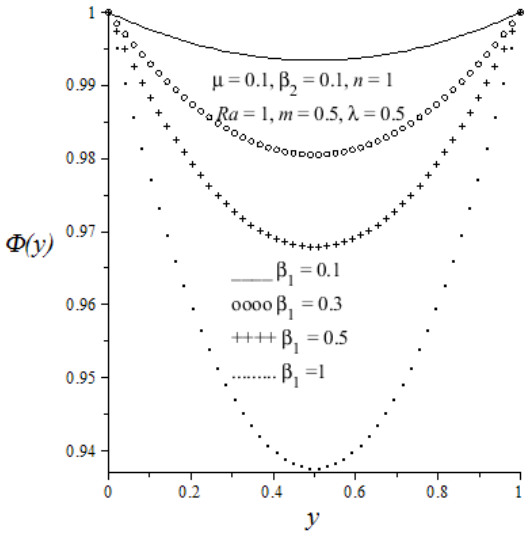

Fig. 12. Effect of increasing β_1 on slab O2 depletion profiles

c) Effects of thermo-physical parameter variation on slab CO_2 emission

Figures 13–18 depict the slab CO2 emission profiles. An increase in the exothermic reaction rate represented by increasing values of λ, leads to an increase in the slab CO2 emission rate as shown in Fig.

13. The emission is highest within the slab centerline region. In Fig. 14, we observe the effect of increasing *Ra* on slab CO2 emission. It can be seen that increasing the value of *Ra* results in the decrease in CO2 profiles. The same scenario was observed with temperature profiles and this is because the more the emissivity of the slab's surface, the lesser O2 depletion and hence the exothermic reaction is assumed to not take place in order to lessen CO2 emission. We observe the same scenario with Fig. 15, where the increase in *n* gives a decrease in CO2 profiles. It is therefore necessary to increase the order of reaction in order to lessen the emission of CO2. Figure 16 illustrates the effect of *m* on CO2. We observe that an increase in *m* corresponds to an increase in CO2 emission profiles and the highest profile is observed during bimolecular reactions (m = 0.5). From Fig. 17 we can see that increasing β_1 decreases the CO2 profiles. The reason is that as more O2 is consumed, the exothermic reaction is reduced and hence the emission of CO2 is lessened. Effects of increasing β_2 on slab CO2 emission profiles are illustrated in Fig. 18. In this case an increase in β_2 corresponds to an increase in CO2 profiles. The presence of more CO2 within a reactive slab reduces the exothermic chemical reaction. During this process O2 is not used up and thus temperature rise together with CO2 emission cannot take place.

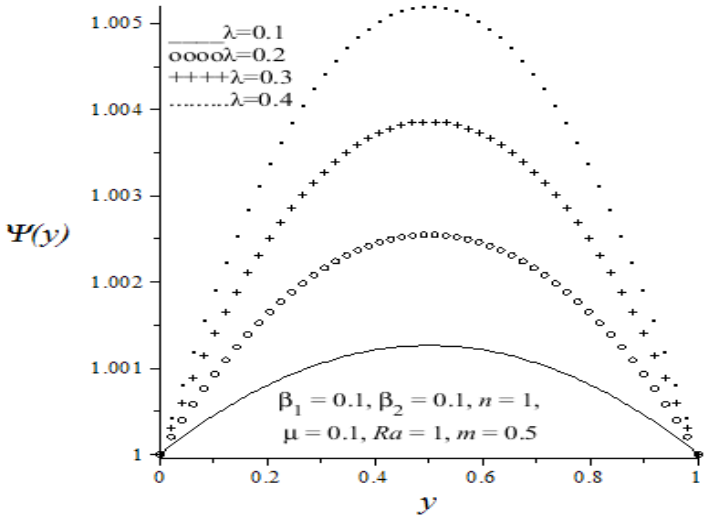

Fig. 13. Effect of increasing λ on slab CO2 emission profiles

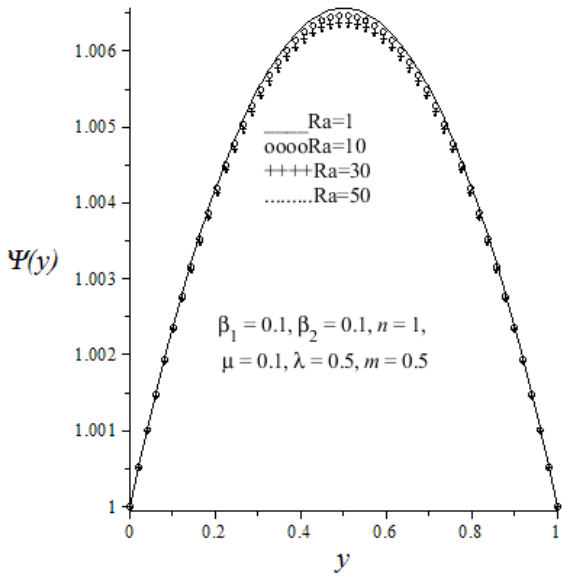

Fig. 14. Effect of increasing *Ra* on slab CO2 emission profiles

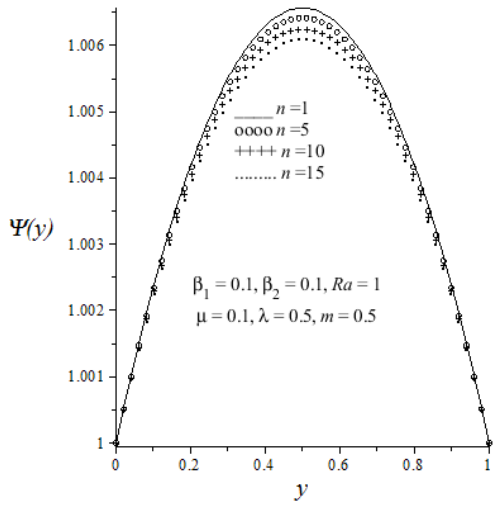

Fig. 15. Effect of increasing *n* on slab CO2 emission profiles

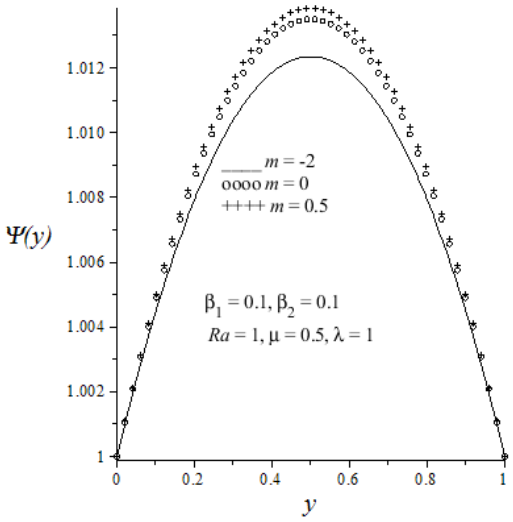

Fig. 16. Effect of *m* on slab CO2 emission profiles

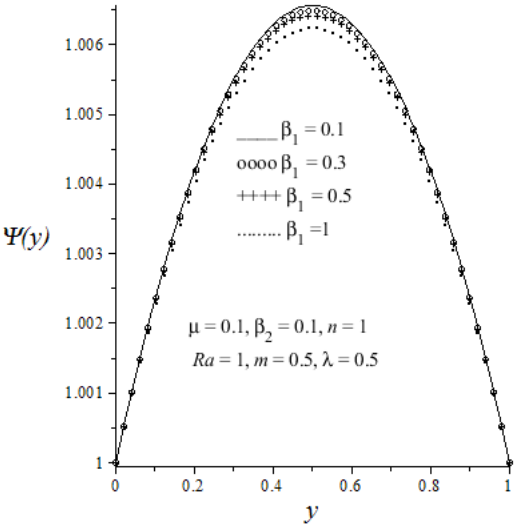

Fig. 17. Effect of increasing β_1 on slab CO2 emission profiles

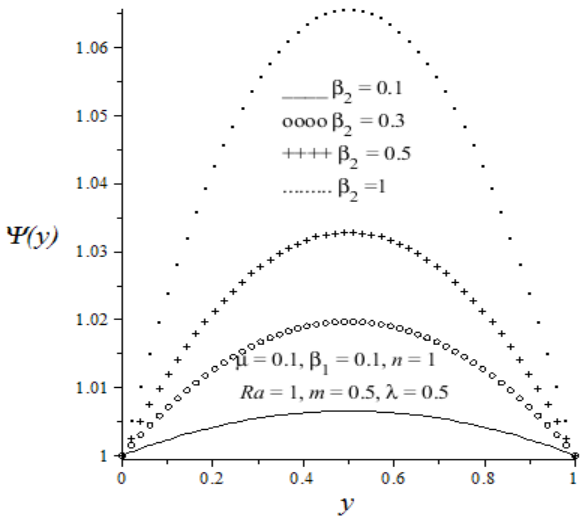

Fig. 18. Effect of increasing β_2 on slab CO2 emission profiles

d) Effects of parameter variation on thermal criticality values or blowups

Here we consider plots for thermal criticality values, Nusselt number *Nu*, versus the rate of reaction, Frank-Kamenetskii parameter λ. We consider manipulating parameters to establish values to help us control the system against any explosion. Results are also presented in a table.

Figure 19 shows that at lowest values of *Ra*, the system blow up values are arrived at quicker, as the rate of reaction increases. It can be seen that at high values of *Ra*, the blow up values are high and therefore it is better to allow more radiation to occur in order to avoid explosions. Figure 20 shows the same scenario, where an increase in *n* enhances thermal stability as the rate of reaction increases. A different picture is shown by Fig. 21. In this case we observe that as *m* increases, the system becomes thermally unstable because at high values of *m*, blow up values are arrived at quicker. Figure 22 illustrates that increasing μ may lead to some thermal stability, because the blow ups occur at high values of rate of reaction as μ increases. Numerical values confirm graphical solutions and are given in Table 1.

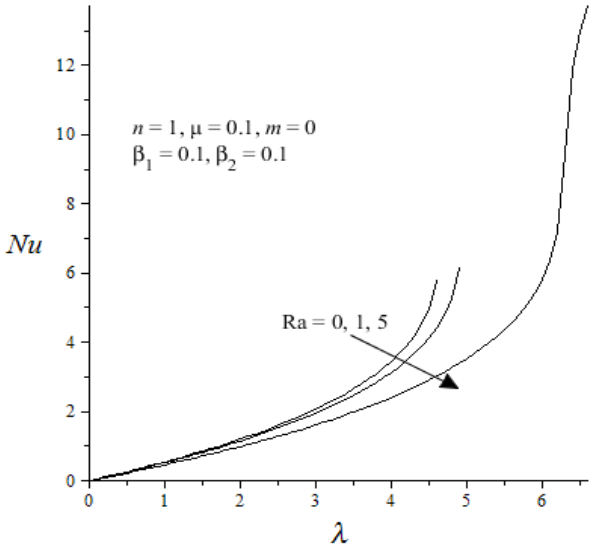

Fig. 19. Effect of increasing *Ra* on slab thermal criticality values

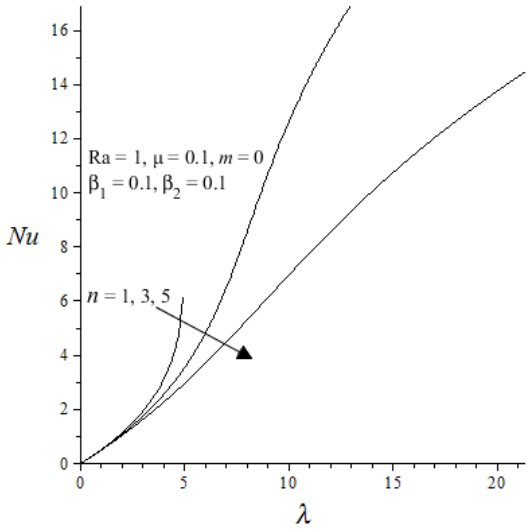

Fig. 20. Effect of increasing n on slab thermal criticality values

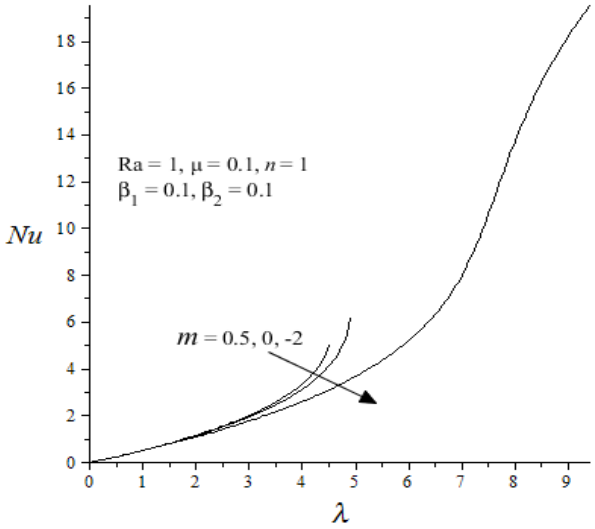

Fig. 21. Effect of m on slab thermal criticality values

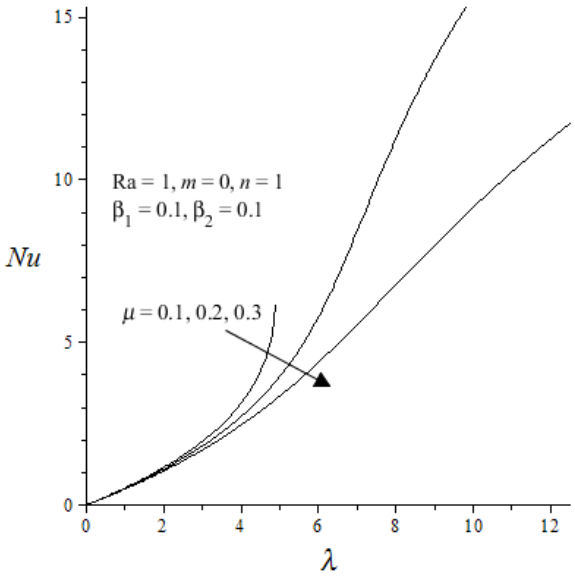

Fig. 22. Effect of increasing μ on slab thermal criticality values

Table 1. Computations showing the effects of various thermo-physical parameters on thermal criticality values. We consider $\beta_1 = \beta_2 = 0.1$

m	Ra	n	μ	Nu	λ_c
-2	1	1	0.1	19.7873	9.4878
0	1	1	0.1	6.4966	4.9129
0.5	1	1	0.1	5.8275	4.5581
0	0	1	0.1	6.2069	4.6195
0	5	1	0.1	13.7238	6.6014
0	1	3	0.1	16.9694	12.9801
0	1	5	0.1	14.4564	21.3100
0	1	1	0.2	15.3221	9.8132
0	1	1	0.3	11.8179	12.5963

5. CONCLUSION

In this paper the impact of heat loss due to radiation on CO_2 emission, O_2 depletion and thermal stability in a reactive slab was observed. From the results obtained, the general trend is that processes which increase both the temperature and CO_2 emission profiles increase the depletion of O_2 in a reactive slab. The thermo-physical parameters identified to lessen CO_2 emission in an exothermic reaction are n, Bi_1, Bi_2, Bi_3, β_1, Ra and μ. Moreover, parameters which help to achieve thermal stability within a stockpile of combustible material have also been identified as Ra, n, and μ. Differential equations governing the problem were obtained and solved numerically using Runge-Kutta-Fehlberg method coupled with shooting technique. Results were shown graphically and discussed accordingly. Measures to control the exothermic reaction taking place in a slab from explosion were considered and results were given graphically and numerically. Using the same derived non-linear differential equations, the investigation can be extended to cylindrical vessels with coordinates, say, (z, r, θ) and also spherical vessels with (r, θ, ϕ) as coordinates.

NOMENCLATURE

m Numerical exponent
n Order of reaction
T Absolute temperature of the slab (K)
T_w Surface temperature of the slab (K)
C O2 concentration ($kgmol^{-1}$)
C_w O2 concentration at the slab surface ($kgmol^{-1}$)
P CO2 concentration ($kgmol^{-1}$)
P_w CO2 concentration at the slab surface ($kgmol^{-1}$)
D O2 diffusivity in the slab
γ CO2 diffusivity in the slab
k Thermal conductivity of the reacting slab ($Js^{-1}m^{-1}K^{-1}$)
$\bar{y}$ Slab rectangular distance (m)
Q Heat of reaction (Jkg^{-1})
$\boldsymbol{A}$ Rate constant (s^{-1})
E Activation energy ($Jmol^{-1}$)
R Universal gas constant ($JK^{-1}mol^{-1}$
l Planck number (Js)
K Boltzmann constant (JK^{-1})
Ra Radiation parameter
Nu Nusselt number
Sh_1 Dimensionless O2 transfer rate at slab's surface
Sh_2 Dimensionless CO2 transfer rate at slab's surface

Greek Symbols

v Vibration frequency (s^{-1})

ε Emissivity of the slab
σ Stefan-Boltzmann constant (W/m^2K^4)
θ Dimensionless temperature
Φ Dimensionless O2 concentration
Ψ Dimensionless CO2 concentration
λ Modified Frank-Kamenetskii parameter
μ Dimensionless activation energy parameter
β_1 O2 consumption rate parameter
β_2 CO2 emission rate parameter

REFERENCES

1. Quick, J. C. & Glick, D. C. (2000). Carbon dioxide from coal combustion: variation with rank of US coal. *Fuel*, Vol. 79, No. 7, pp. 803–812.
2. Betz, R. & Sato, M. (2006). Emissions trading: lessons learnt from the 1st phase of the EU ETS and prospects for the 2nd phase. *Climate Policy*, Vol. 6, No. 4, pp. 351–359.
3. Bebernes, J. & Eberly, D. (1989). Mathematical problems from combustion theory. *Applied Mathematical Sciences*, Vol. 83, Springer, New York, NY, USA.
4. Williams, F. A. (1985). *Combustion Theory*. Benjamin & Cuminy Publishing, Menlo Park, Calif, USA, 2nd edition.
5. Quadrelli, R. & Peterson, S. (2007). The energy-climate challenge: recent trends in GHG emissions from fuel combustion. *Energy Policy*, Vol. 35, N0. 11, pp. 5938–5952.
6. Planck, M. (1988). *The theory of heat radiation*. The history of modern physics 1800–1950, Vol. 11. New York: Tomash Publishers – American Institute of Physics.
7. Cheng, P. (1964). Two dimensional radiating gas flow by a moment method. *A I A A J.*, 2, 1662-1664.
8. Isvoranu, D. B. & Badescu, V. (2008). Radiation exergy: the case of thermal and nuclear energy. *International Journal of Nuclear Governance, Economy and Ecology*, Vol. 2, No. 1, pp. 90–112.
9. Liao, S., Su, J. & Chwang, A. T. (2006). Series solutions for a nonlinear model of combined convective and radiative cooling of a spherical body. *International Journal of Heat and Mass Transfer*, Vol. 49, pp. 2437–2445.
10. Tan, Z., Su, G. & Su, J. (2009). Improved lumped models for combined convective and radiative cooling of a wall. *Applied Thermal Engineering*, Vol. 29, pp. 2439–2443.
11. Siegel, R. & Howell, J. R. (1981). *Thermal radiation heat transfer*. New York: Hemisphere Publishing Corporation.
12. J. M. Simmie, J. R. (2003). Detailed chemical kinetic model for the combustion of hydrocarbon fuels. *Prog. Energy Combust. Sci.*, Vol. 29, pp. 599634.
13. Dainton, F. S. (1960). *Chain reaction: An introduction*. Wiley, New York, NY, USA.
14. Frank-Kamenetskii, D. A. (1969). *Diffusion and heat transfer in chemical kinetics*. Plenum Press, New York.
15. Makinde, O. D. (2004). Exothermic explosions in a Slab: A case study of series summation technique. *International Communications in Heat and Mass Transfer*, Vol. 31, No. 8, pp. 1227-1231.
16. Sadiq, M. A. & Merkin, J. H. (1994). Combustion in a porous material with reactant consumption: the role of the ambient temperature. *Mathematical and Computer Modelling*, Vol. 20, No. 1, pp. 27–46.
17. Legodi, A. M. K. & Makinde, O. D. (2011). A numerical study of steady state exothermic reaction in a slab with convective boundary conditions. *International Journal of the Physical Sciences*, Vol. 6, No. 10, pp. 2541-2549.
18. Makinde, O. D., Chinyoka, T. & Lebelo, R. S. (2011). Numerical investigation into CO_2 emission, O_2 depletion and thermal decomposition in a reacting slab. *Mathematical Problems in Engineering*, Vol. 2011, 208426, pp. 1-19.
19. Makinde, O. D. (2012). Hermite-Padé approach to thermal stability of reacting masses in a slab with asymmetric convective cooling. *Journal of the Franklin Institute*, Vol. 349, pp.957-965.

20. Makinde, O. D. (2012). On the thermal decomposition of reactive materials of variable thermal conductivity and heat loss characteristics in a long pipe. *Journal of Energetic Materials*, Vol. 30, pp. 283-298.
21. Mathews, J. H. & Fink, K. D. (1999). *Numerical methods using matlab*. 3rd edition. Prentice Hall.